Nanoscale

Accepted Manuscript

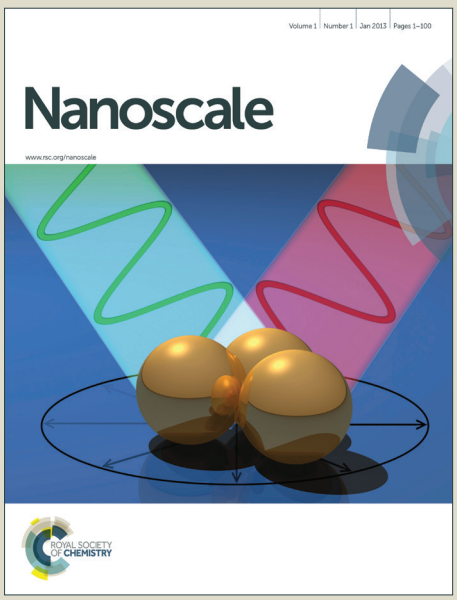

ROYAL SOCIETY OF CHEMISTRY

www.rsc.org/nanoscale

Fabrication of Bright and Small Size Semiconducting Polymer Nanoparticles for Cellular Labelling and Single Particle Tracking

*Lin Wei, Peng Zhou, Qingxiu Yang, Qiaoyu Yang, Ming Ma, Bo Chen, and Lehui Xiao**

Key Laboratory of Chemical Biology & Traditional Chinese Medicine Research, Ministry of Education, Key Laboratory of Phytochemical R&D of Hunan Province, College of Chemistry and Chemical Engineering, Hunan Normal University, Changsha, Hunan, 410081, P. R. China.

KEYWORDS

semiconducting polymer, polymer nanoparticles, fluorescent nanoparticles, single particle tracking, cellular labelling

ABSTRACT

In this work, we demonstrated a convenient and robust strategy for the efficient fabrication of high fluorescence quantum yield (QY, 49.8%±3%) semiconducting polymer nanoparticles (SPNs) with size comparable to semiconductor quantum dots (Qdots). The SPNs were synthesized by co-precipitation of hydrophobic semiconducting polymer together with amphiphilic multidentate polymer. The comprehensive spectroscopic and microscopic characterizations illustrate that the SPNs possess superior photophysical performances such

as excellent fluorescence brightness, reduced photoblinking in contrast to Qdots, as well as good photostability over similar size fluorescent protein, phycoerythrin. More importantly, by conjugating membrane biomarkers onto the surface of SPNs, it was found that they were not only applicable for specific cellular labelling but also suitable for single particle tracking due to the improved optical performances.

INTRODUCTION

Development of optical imaging contrast reagents with noble photophysical and biological functionality has aroused ongoing interest over past decades. With the help of optical microscopic imaging tools, the mechanisms of many intriguing yet mysterious biological or chemical processes have been successfully elucidated based on those probes. Currently, the most widely adopted fluorescent contrast reagents include small organic dyes, fluorescent proteins, carbon nanomaterials as well as inorganic nanomaterials (e.g. Qdots).[1-9] Due to the restricted photochemical stability, the former two only generate limited photons before the photobleaching process. Therefore, they are not suitable for sensitive analysis and long-term dynamic observation.[10-12] The carbon nanomaterials (such as nanotube and nanodots) have improved optical stability but still suffer to the limitation of extremely low QY (usually less than 1%) and poor solubility in physiological surroundings.[7, 13, 14] As a consequence, they are more often adopted as versatile fluorescence quenchers and photo-thermal transducers.[15, 16] Qdots exhibit better photochemical stability and improved fluorescence QY; however, the inherent frequent transitions between “on” and “off” states together with the less-desirable biocompatibility greatly limits their in-vivo applications.[2, 17, 18]

The recently developed fluorescent semiconducting polymer nanoparticles (SPNs) open a new avenue to address above challenges.[19-23] The design is based on the water

solubilization of hydrophobic semiconducting polymers that are typically composed of π-conjugated backbones. The delocalized π electrons on the backbone of the semiconducting polymer will give rise to π- π^* electron transitions in the presence of favorable stimulation, which can then generate excitons for photo luminescence.[24] Through tuning the length of the conjugated backbone and manipulating the chemical structure of the side chains, the absorption and emission band of conjugated polymer can be readily modified over broad wavelengths. In contrast to individual organic dyes, conjugated polymers exhibit superior photostability and brilliant fluorescence, which make them potentially suitable for fluorescence-based ultrasensitive diagnosis.[21, 23-26]

So far, several methods (such as reprecipitation and miniemulsion) have been reported to fabricate water-soluble nanometer-sized polymer dots and have demonstrated their preliminary capability in biological imaging.[19, 23, 25, 27] Nevertheless, the SPNs prepared by those strategies are typically with limited colloidal stability in physiological solution, reduced fluorescence QY as well as relatively large hydrodynamic size (tens of or even hundreds of nanometer). For biological applications, the large hydrodynamic size will adversely affect the specific molecular binding and in-vivo biodistribution.[28-30] Therefore, exploration of versatile strategies for the fabrication of small size and bright SPNs is highly desired. On this basis, Hashim et. al. used polyethylene glycol as the stabilizing ligand and successfully synthesized small size SPNs with diameter less than 5 nm.[22] However, a major limitation of this method is that the fluorescence QY (around 10% for F8BT) of the SPNs is typically very low and it is difficult to further functionalize the SPNs with biological molecules owing to the lacking of functional group on the nanoparticle surface.

In this study, we demonstrate a convenient and robust one-pot strategy for the efficient fabrication of water-soluble and small size poly[(9,9-dioctylfluorenyl-2,7-diyl)-alt-co-(1,4-

benzo-(2,1',3)-thiadiazole)] (PFBT) SPNs with significantly enhanced fluorescence QY. The comprehensive spectroscopic and microscopic characterizations illustrate that the as-prepared SPNs display improved photophysical performance not only in the bulk state but also at single particle level in comparison with fluorescent dyes, Qdots, and fluorescent protein. The specific tumor cell labelling experiments further indicate that the bioconjugated SPNs represent superior biological labelling performance over the commonly adopted fluorescent protein, phycoerythrin. In addition, the time-resolved single particle tracking experiments on living cell membrane also verify that these SPNs are not only suitable for ultrasensitive biological diagnosis but also good candidates for fast dynamic events tracking at single particle level in living cells.

RESULTS AND DISCUSSION

Fabrication of SPNs.

The PFBT SPNs were synthesized based on a modified co-precipitation method, which takes the advantages of reprecipitation and mini-emulsion methods.[19, 23] Scheme 1 depicts the basic principle of this method where amphiphilic multidentate polymer was firstly mixed with the semiconducting polymer in tetrahydrofuran (THF). Quick injection of the mixture into water in a sonication bath will result in emulsified nanodroplets. The amphiphilic multidentate polymer was fabricated by grafting dodecylamine (DDA) and mercaptoethylamine (MEA) onto the poly(acrylic acid) (PAA, Mw~2,000) backbone through carboxylic acid and amine linkage. Detailed procedures are described in the supporting information. Since the PAA polymer is nearly insoluble in THF, it is impossible to directly synthesize small size water-soluble SPNs through co-precipitation of semiconducting polymer with PAA. Partially covalent conjugation of DDA to carboxylic acids on the backbone of PAA can generate an amphiphilic multidentate polymer which is soluble not

only in THF but also in water. In contrast to the previously reported strategies, one of the essential merits of this design is that, when the multidentate polymer solution (in THF) was dispersed in water together with semiconducting polymers, the amphiphilic polymer could assemble into a close configuration which contains a compact hydrophobic core and a negatively charged hydrophilic polymer shell.[31] The compact and stable hydrophobic core can keep the semiconducting polymer away from oxidative reagents as well as other reactive molecules. It therefore greatly reduces the probability of photochemical reactions in complex biological environments.

For quantum-sized nanoparticles (e.g., Qdots and metal clusters), photoblinking is a common yet undesirable phenomenon that seriously degrades the optical performance. It was found that introducing triplet state quencher (e.g., mercaptoethylamine) to the buffer solution could greatly suppress the probability of "on" and "off" transitions and increase the fluorescence intensity simultaneously.[32, 33] However, a limitation of this design is that, in order to achieve satisfactory suppression effect, a relatively high concentration of triplet state quencher is typically required (>10 mM), which is not compatible in some particular cases, such as inside living cells. In this regard, we integrated MEA directly into the amphiphilic polymer and anticipated that the locally increased content of MEA would play a complementary role on the improvement of the optical performance. Meanwhile, the remained carboxyl groups exposed on the surface of the SPNs afford a versatile platform for the facile conjugation of additional functional biomolecules.

Spectroscopic Characterizations of SPNs.

Currently, poly(styrene-co-maleic anhydride) and poly(styrene)-block-poly(ethylene glycol)) are two commonly adopted phase transfer reagents for the fabrication of SPNs.[19, 21] The size of SPNs made by those ligands is usually as large as tens of nanometer and it is

accompanied with greatly reduced fluorescence QY in comparison with their corresponding constituents in organic surroundings. One of the major reasons for the drastic fluorescence decreasing is that the tight and direct aggregation of semiconducting polymers from the random coil structure to the form of compact sphere will cause non-radiative species across the polymer chain, for example excimers, aggregates and defects.[34, 35] On the other hand, the direct exposure of the semiconducting polymer to the polar solvent would be another source for the quenching effect (i.e. solvent effect).

In the present study, these two issues are compromised by using the new synthesized amphiphilic multidentate polymer. During the co-precipitation process, the amphiphilic polymers would wrap around the surface of the THF nano-droplet with alkane chains penetrating inside the hydrophobic core. Although evaporation of THF solution can further shrink the droplet into a compact nano-dots, it is distinct from the previously reported designs that the semiconducting polymers embedded in the hydrophobic core are intercalated by alkane chains (i.e., dodecylamine). The interchain or intrachain π-orbital stacking can thus be effectively suppressed, which is revealed in the corresponding fluorescence spectra where a 3 nm blue-shift is observed, Figures S1. It should be noted that the balance composition of DDA, MEA and carboxylic acids on the backbone of PAA could greatly affect the optical performance of the SPNs, Figure 1. Increasing the percent of DDA, the fluorescence intensity of SPNs increased simultaneously. A plateau was observed when the percent of DDA reached 40%. Meanwhile, introducing MEA to the structure of PAA indeed improves the fluorescent performance of SPNs not only at ensemble scale but also at single particle level, Figure S2. In the optimum condition (40% DDA, and 5% MEA), the fluorescence intensity of the SPNs is generally enhanced more than two times over those without ligand modification under the same mass concentration. This result is generally consistent with the QY measurements where the QY of these SPNs (49.8%±3%) is roughly three times higher over

those regular polymer nanoparticles (17%) without multidentate polymer coating. The measured fluorescence lifetime of SPNs is around 3.2±0.2 ns, which is slightly shorter than the typical fluorescence lifetime of semiconducting quantum dots (tens of nanoseconds).

The Size and Stability of SPNs.

For biological applications, the hydrodynamic diameter of fluorescent nanoparticles is one of the most important criteria for the evaluation of their biological performance because it not only affects their dynamic kinetics in the complex and crowding cellular environment but also influences the biological activity of the functional molecules tagged on the surface.

The hydrodynamic size of the SPNs is determined by dynamic light scattering (DLS). Figure 2 shows the representative DLS result of the high QY SPNs in deionized water. Remarkably, the measured hydrodynamic diameter is as small as 4.7±1.3 nm, which is even smaller than that of commercially available water-solubilized Qdots. Generally, for a Qdots with core size around 4-5 nm, the hydrodynamic size will reach to 20-40 nm.[28, 31, 36, 37] One of the major reasons for the increased hydrodynamic size is that the phase transfer reagents are usually coated on the primary ligand layer (hydrophobic) directly, leading to a loosely covered polymer shell. In this work, due to the flexibility of the semiconducting polymer, the alkane chains of the amphiphilic phase transfer can directly penetrate into the semiconducting polymer core, which can thus afford two important merits for the as-synthesized SPNs. One is the condensed hydrodynamic size as demonstrated above. The other is the good colloidal stability, which will be discussed as below.

To ascertain the DLS result, we performed TEM measurement for the SPNs. As shown in Figure 2, the SPNs represent narrow size distribution in the TEM image that is well in line with the DLS measurement. It is worthy of note that the size the SPNs from the TEM result (3.1±0.4 nm) is slightly smaller than the hydrodynamic diameter determined by DLS.

Considering the different sample states as well as the detection mechanisms between these two detection schemes, this discrepancy is satisfactory because the size characterized by TEM is from the particles in a dried state on solid surface. The water evaporation process might further affect the size of the SPNs.

Typically, the stability of fluorescent nanoparticles in solution is characterized by two aspects. One is the colloidal stability against aggregation, which can be revealed by zeta potential. The value of -31.1±2.5 mV from these SPNs indicates that they would be stable enough to suffer the harsh physiological environment and complex salt solutions. This argument was validated by stability analyses in different surroundings such as different ionic strengths, pH values and inside cell culture medium with serum, Figure 3. The other one is the stability of the phase transfer molecules against dissociation. As discussed above, because of the intercalated net structure, the multidentate polymer should be difficult to spontaneously dissociate away from the nano-composite. This design is obviously superior to the small surfactant molecules applied in mini-emulsion scheme. To ascertain this point, we continuously monitored the fluorescence intensity of the SPNs for one week, Figure 3c. No fluctuation was observed, confirming the compact and stable structure of these SPNs.

It is worthy of note that the fluorescence spectrum of the SPNs is insensitive to the size dependent quantum confinement effect.[21, 24, 38] As a consequence, one can readily manipulate the emission wavelength of the SPNs by changing the chemical structure of the semiconducting polymer while still maintaining a small hydrodynamic size. This feature is especially important for biological applications and is hardly accessible by Qdots whose emission wavelength is typically size dependent.

Besides the size and QY, another essential factor for the characterization of the fabrication strategy is the product yield. Based on the fluorescence spectroscopic estimation,

the product yield of these SPNs is as high as 96±2.7%. The high product yield might be mainly benefitted from the facile fabrication procedures. A recent report has also demonstrated the successful fabrication of water-soluble SPNs with size comparable to Qdots; however, the drastically reduced fluorescent QY makes those SPNs hardly accessible for biological imaging applications.[22] More importantly, no biological functional group is available from those SPNs, thus grafting of functional biomolecules to their surface becomes a huge challenge.

The Optical Performance at Single Particle Level.

From the consideration of biological imaging applications, it is practically more interesting to evaluate the photophysical performance of SPNs at single particle level in comparison with comparable size fluorescent materials, such as Qdots and fluorescent proteins. It is well known that the fluorescent brightness of individual object is mainly determined by the product of two items, i.e., the fluorescence QY and the absorption cross-section. The estimated single particle absorption cross-sections of SPNs is around 3.9×10^{-14} cm^2. Typically, for a Qdots and fluorescent protein phycoerythrin, the reported optical cross-sections are on the order of 4.5×10^{-15} and 9×10^{-15} cm^2 respectively.[39, 40] Therefore, the estimated brightness from single PFBT SPNs would be roughly 10 and 2.6 times brighter than single Qdots and phycoerythrin respectively. As shown in Figure 4a, a set of single particle (molecule) fluorescence imaging experiments were conducted. The fluorescent spots from all of the CCD images are dispersed separately on the glass slide surface, indicative of what we observed are individual objectives. Notably, from the statistical single particle fluorescence intensity analyses, the SPNs show the brightest intensity among those controls, i.e. eight and two times brighter than Qdots and single phycoerythrin respectively under the same imaging conditions, Figure 4b. These values indicate that the single particle microscopic brightness analyses are in good agreement with the spectroscopic estimations.

To further understand the photo-stability of the SPNs, we performed time-resolved single particle fluorescence intensity analysis. Representative fluorescence intensity fluctuation tracks from single objects are shown in Figure 4c. Majority of the fluorescent proteins were photo-bleached less than 10 s. Qdots represent relatively better photo-stability; however, as evident in the fluorescence intensity tracks, inherent serious "on" and "off" transitions dominate the whole track which is a significant roadblock in biological imaging at single particle level. Similar fluorescence blinking effect from phycoerythrin can also be found in the time-dependent intensity track. On the contrary, the individual SPNs shows noticeably improved photostability on photo luminescence during the whole observation window, which will facilitate the continuous observation of fast dynamic events without loss of any critical transient states. It is important to note that the SPNs are basically composed by relatively biocompatible organic polymers, Figure S3. As a consequence, based on the above comprehensive spectroscopic and microscopic characterizations, we can envision that the SPNs are potentially more suitable for biological imaging due to the improved photophysical property over traditional fluorescence contrast reagents.

Cellular Labelling and Single Particle Tracking with SPNs.

To demonstrate the biological imaging versatility of these SPNs, we conducted specific tumor cell targeting as well as single particle tracking on living cell membrane. For the tumor cell recognition experiment, we firstly conjugated the SPNs with streptavidin via EDC/Sulfo-NHS. A successful crosslinking procedure should then contribute increased hydrodynamic size for the nano-composite. As expected, after the bioconjugation process, around 2.6 nm increment in the DLS measurement was readily observed, Figure S4. Because of the strong streptavidin/biotin association, the functionalized SPNs can then be effectively and specifically labeled on the membrane of target MCF-7 breast cancer cells in the presence of biotinylated monoclonal epithelial cell adhesion molecule (EpCAM) antibody whose receptor

is widely adopted for the detection of circulating tumor cells. Figure 5 shows the representative fluorescent images of tumor cell targeting experiments. The well-defined circular fluorescent profiles from all of cells in Figure 5a indicate that the bioconjugated SPNs can effectively target on the specific cell membrane in the presence of monoclonal antibody. Non-specific binding with other membrane proteins was not observed as demonstrated by the negative control, which is also in good agreement with the relatively homogeneous fluorescence distribution on the positive cell membranes. The intracellular non-specific adsorption can also be ruled out based on the 3D Z slicing fluorescence images, Figure S5.

In order to evaluate the biological labelling performance of the SPNs, we applied streptavidin conjugated phycoerythrin as the positive control. Interesting, the quantitative statistical fluorescence intensity analyses from individual cells demonstrate that the brightness of the SPNs labeled cell is around 1.5 times stronger than that of phycoerythrin labeled cell under the same monoclonal antibody concentration. It should be noted that slight aggregation induced nonspecific binding from the phycoerythrin labeled cell could be readily found through the 3D Z slicing images, Figure S5. This might be one of the reasons for the weaker fluorescence intensity in the cellular labelling experiments in comparison with that of single particle (molecule) brightness estimations. However, these results still give rise to a clear point that the SPNs are promising candidates for ultrasensitive bio-sensing applications.

To further demonstrate the capability of these SPNs in biological imaging applications at single particle level, we conducted single particle tracking experiment on the living cell membrane. The streptavidin conjugated SPNs were firstly incubated with excessive biotinylated monoclonal EpCAM antibody in PBS buffer for 30 min. 1 μL of this nanocomposite solution was then added to the cell culture dish and incubated for another 5 mins to facilitate the SPNs labeled EpCAM antibody to effectively dock on the cell

membrane. Figure 6 shows the tracking results from individual SPNs. According to the fluorescence image stack, it is evident that the single SPNs shows brilliant fluorescence on the cell membrane despite of the strong self-fluorescence from the living cell. The quantitative time dependent fluorescence intensity analysis illustrates that there is no evident "on" and "off" transitions in the whole observation window, which is a significant benefit for single particle tracking. More importantly, according to the time-resolved signal-to-noise ratio (S/N) track, at most of the time, the S/N is better than 10 (with exposure time of 30 ms). It means that, for quantitative translational tracking, the localization accuracy can be better than 3 nm based on the feature-point-tracking algorithm.[41-43]

CONCLUSION

In the field of fluorescence-based imaging studies, currently, Qdots and fluorescent proteins display the most attractive photo-physical and -chemical properties. For Qdots, due to the large surface-to-volume ratio, many functional materials (e.g., drugs, anti-sense RNA and genes) have been specifically delivered to the subcellular locations for the high efficient therapeutic applications.[44, 45] However, the majority of current Qdots contain toxic materials (e.g. cadmium). In the region of short-term consideration, several studies have found that releasing of cadmium ions by oxidation can damage DNA and be acutely toxic to living cells. Additionally, the more essential issue, the long-term in-vivo biological side effect is still elusive until now.[44]

For fluorescent proteins, although they exhibit brighter photo luminescence over organic dyes or even Qdots, the complicated chemical environments (e.g., pH, ionic strength) in biological system will adversely affect their optical performance during the imaging process.[9] As a consequence, the accurate explanation of vital reaction mechanisms based on the quantitative fluorescence analysis becomes complicated. Moreover, the fast photobleaching

rate and inevitable blinking effect are other grand challenges in single molecule based imaging applications.

The SPNs reported here provide one of the most attractive solutions to the above issues. The detailed spectroscopic and microscopic characterizations verify that the SPNs exhibit high fluorescence QY, improved photostability, easy optical tunability, as well as facile surface chemistry for bioconjugation, which are superior to the current fluorescent dyes, fluorescent proteins and Qdots. Therefore, the small size SPNs would further extend the applications of semiconducting polymers in molecular and cellular imaging at single molecule and single particle level in the near future.

ASSOCIATED CONTENT

Supporting Information. Experimental section and additional supporting results as noted in the text. This material is available free of charge via the Internet at http://pubs.acs.org.

AUTHOR INFORMATION

Corresponding Author

E-mail: lehuixiao@gmail.com

Author Contributions

L. W and P. Z. contribute equally to this work.

Notes

The authors declare no competing financial interests.

ACKNOWLEDGMENT

This work was supported by NSFC (21205037, 20927005 and 21275049) Program for New Century Excellent Talents in University (China, NCET-13-0789), Hunan Natural Science Funds for Distinguished Young Scholar (14JJ1017), and the aid program for science and technology innovation research team in higher education institutions of Hunan Province (2010TT1001).

Figures and captions

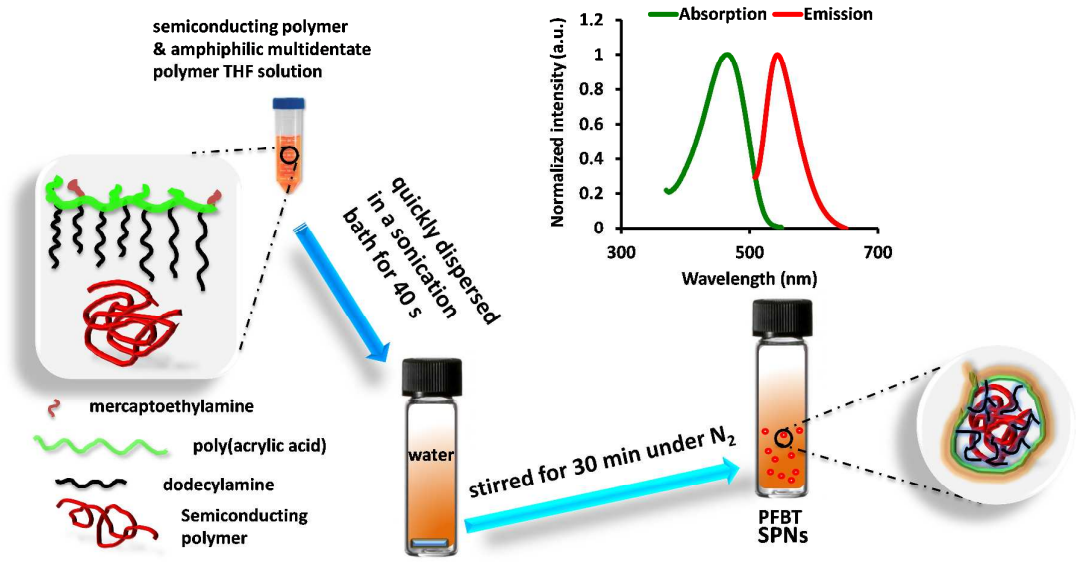

Scheme 1. Schematic diagram for the fabrication of small size and high QY PFBT SPNs.

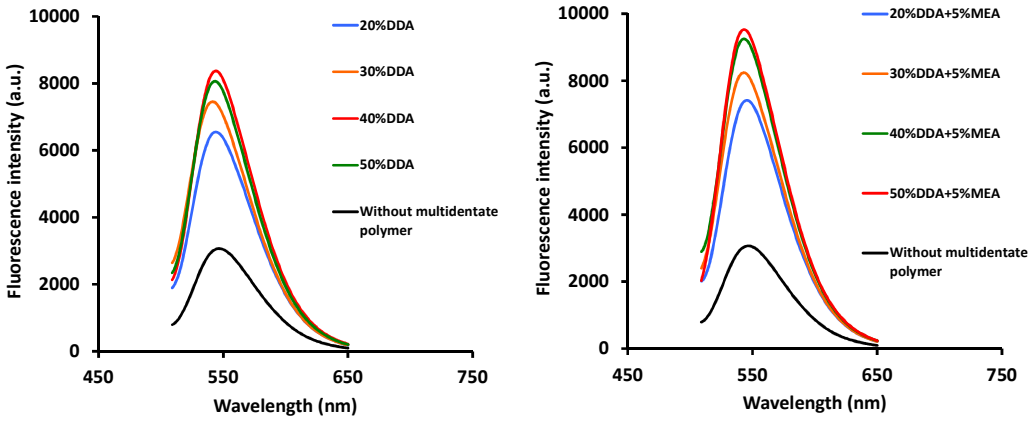

Figure 1. Fluorescence emission spectra of SPNs protected by multidentate polymers with different percent of DDA on the PAA backbone without MEA (left) and in the presence of 5% MEA (right).

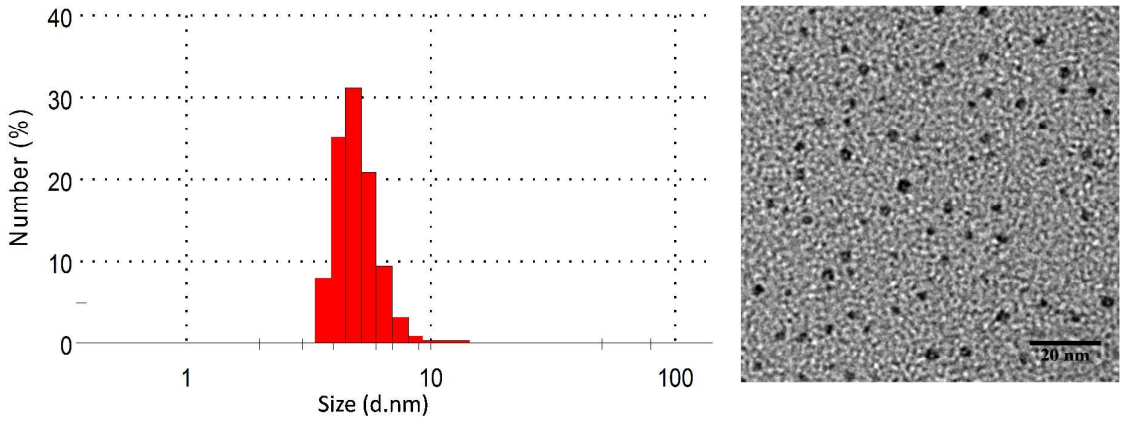

Figure 2. DLS (left) and TEM (right) results of freshly synthesized PFBT SPNs without biological conjugation.

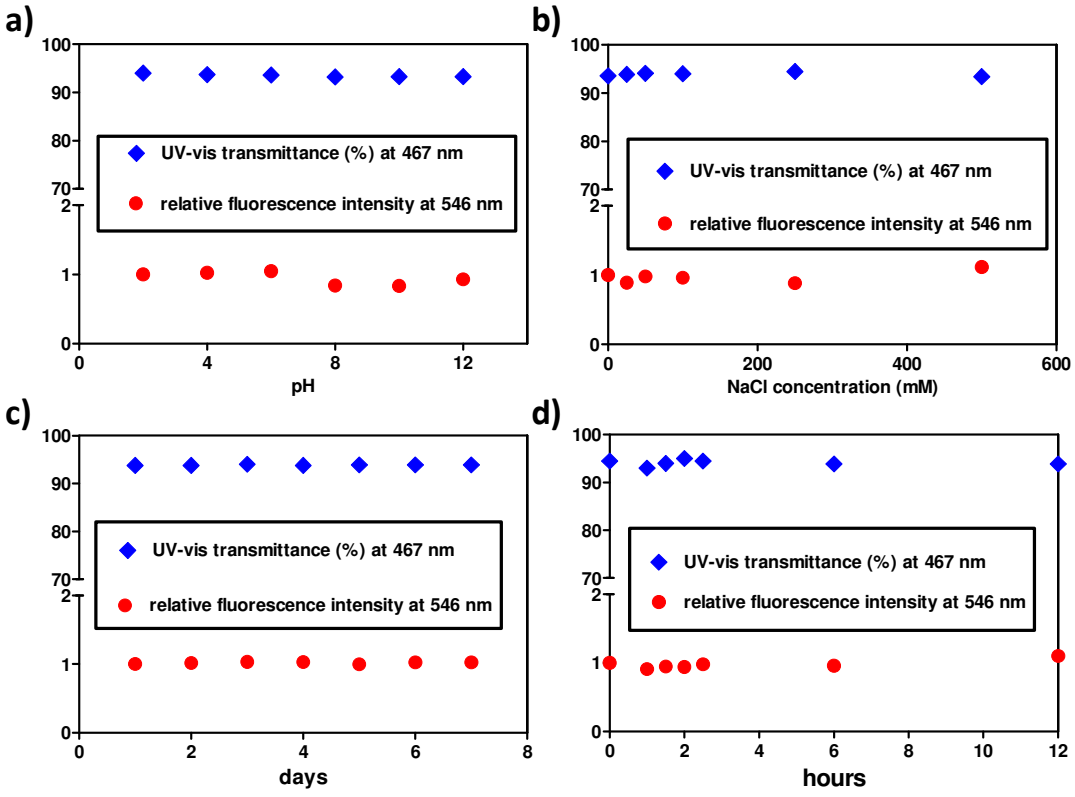

Figure 3. The stability analyses of PFBT SPNs. The UV-vis transmittance (at 467 nm) and the relative fluorescence intensity (at 546 nm) of PFBT SPNs as a function of pH a), NaCl concentration b), the time in DI water c) and the time in cell culture medium with 10% of fetal bovine serum d).

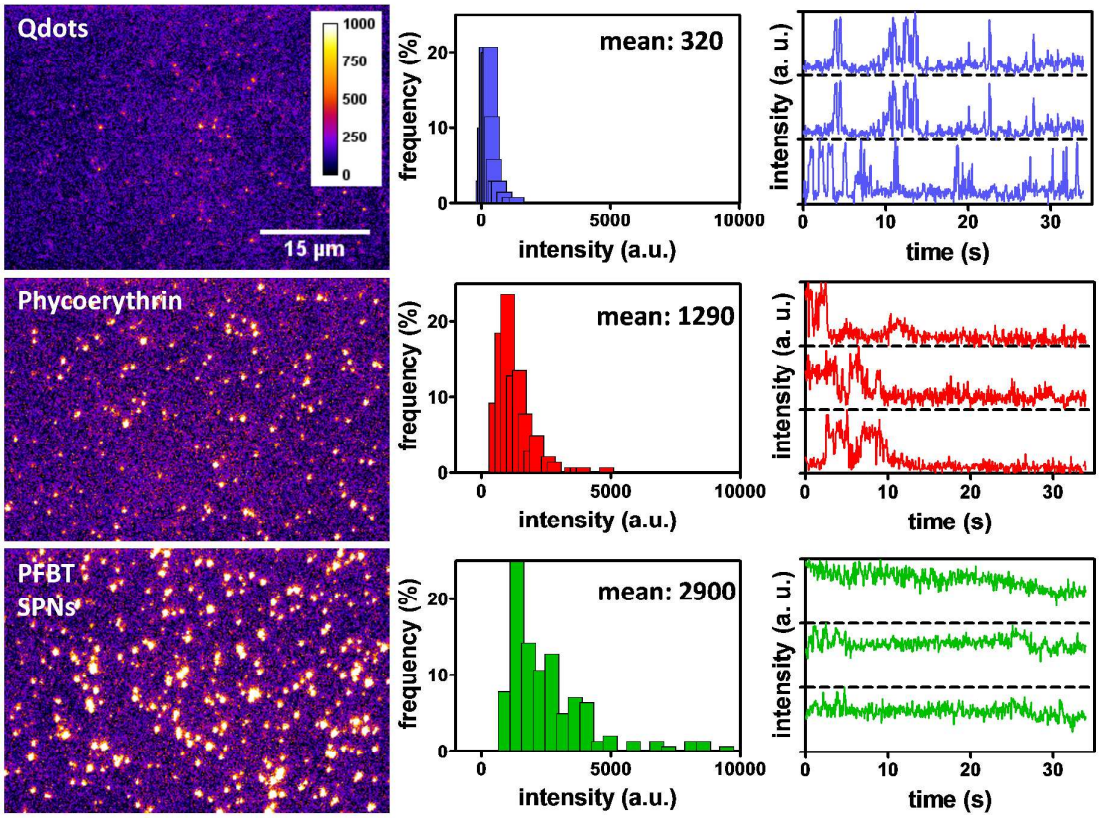

Figure 4. Representative single particle (molecule) fluorescence images of Qdots, phycoerythrin, and PFBT SPNs (left panel). The corresponding intensity distribution histograms of these single objects are shown in the middle panel. Typical fluorescence intensity fluctuation trajectories from individual Qdots, phycoerythrin, and PFBT SPNs are illustrated in the right panel.

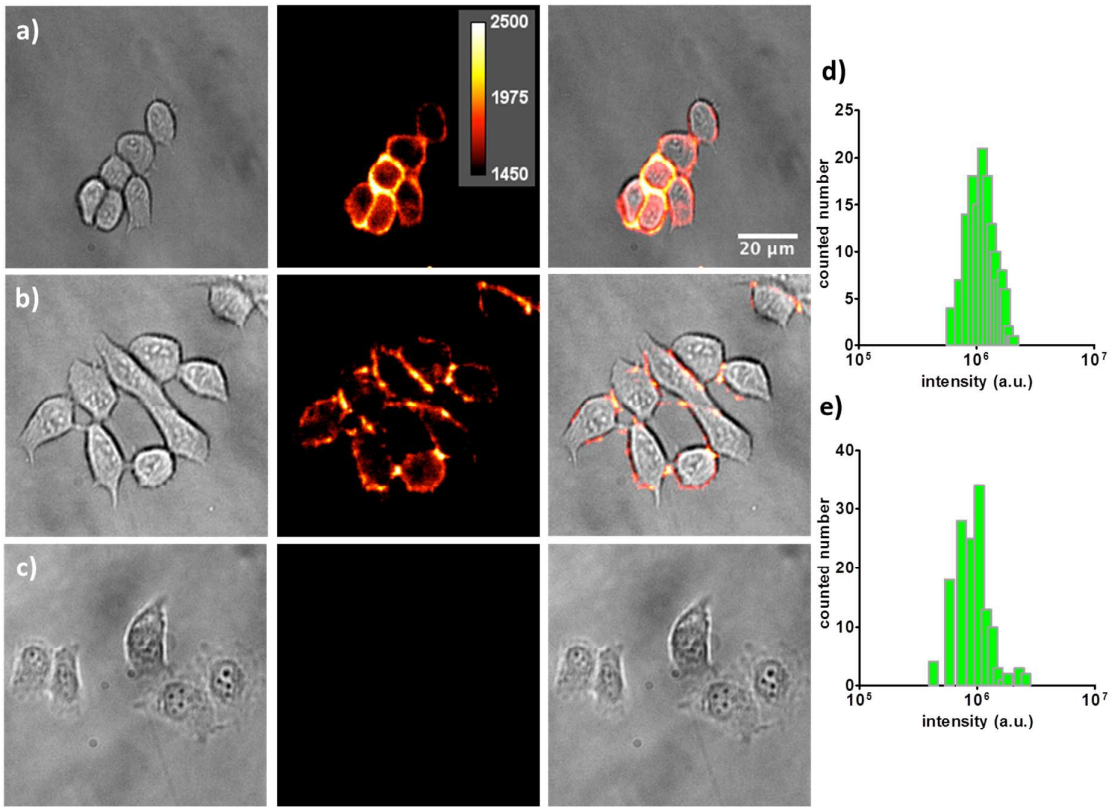

Figure 5. The cellular labelling results. a) the MCF-7 cell membrane labelling results from streptavidin conjugated PFBT SPNs in the presence of biotinylated primary anti-EpCAM antibody. From left to right are the bright-field optical microscopic image, the epi-fluorescence image from PFBT SPNs, and the merged image, respectively. b) the positive control from streptavidin conjugated phycoerythrin. c) the negative control in the presence of streptavidin conjugated PFBT SPNs but without biotinylated primary anti-EpCAM antibody. The statistical single cell fluorescence intensity analyses from PFBT SPNs and phycoerythrin labeled MCF-7 cells are shown in d) and e) respectively. As demonstrated in d) and e), the fluorescence from PFBT SPNs labeled individual MCF-7 cell is around 1.4 times brighter than that from phycoerythrin labeled cell.

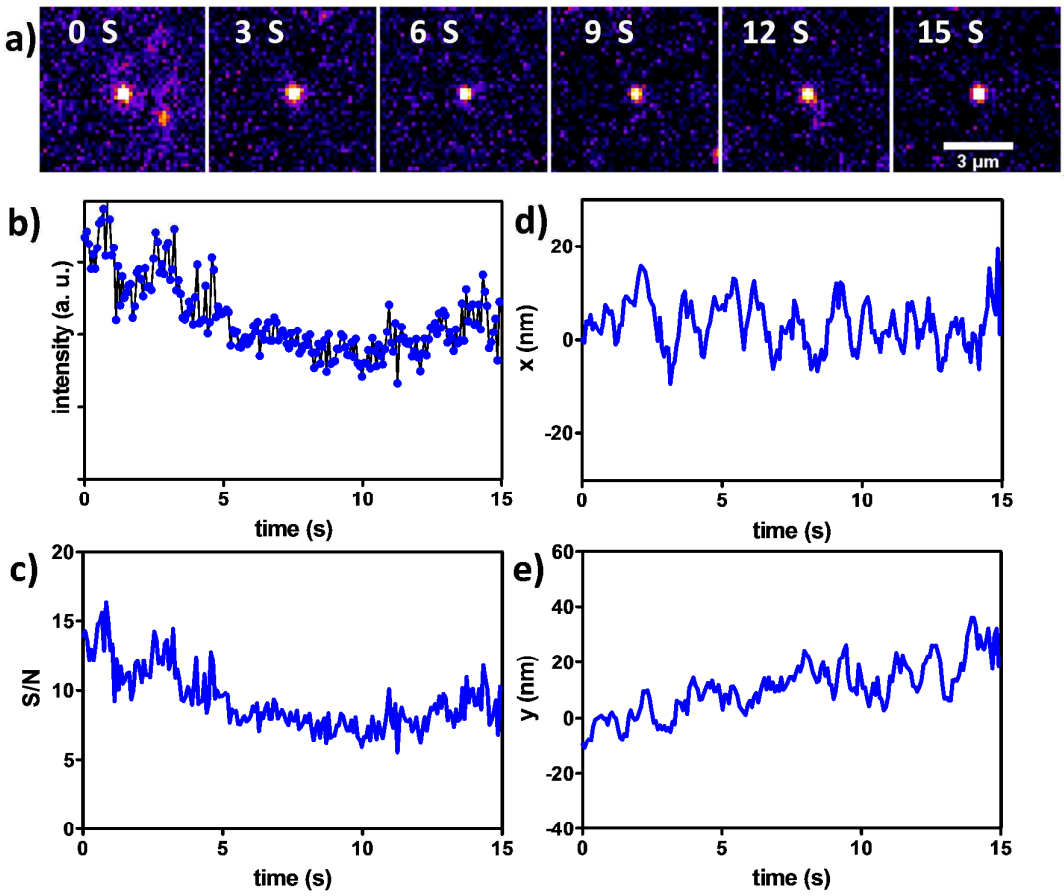

Figure 6. The single particle tracking results. a) the time dependent fluorescence images of single PFBT SPNs on living cell membrane. The fluorescence intensity track, S/N track, and translational diffusion positions in x and y directions from this SPNs within 15 s are shown in b), c), d) and e) respectively.

REFERENCES

1. J. Zhang, R. E. Campbell, A. Y. Ting and R. Y. Tsien, *Nat. Rev. Mol. Cell Bio.*, 2002, 3, 906-918.
2. X. Michalet, F. F. Pinaud, L. A. Bentolila, J. M. Tsay, S. Doose, J. J. Li, G. Sundaresan, A. M. Wu, S. S. Gambhir and S. Weiss, *Science*, 2005, 307, 538-544.
3. A. P. Alivisatos, W. W. Gu and C. Larabell, *Annu. Rev. Biomed. Eng.*, 2005, 7, 55-76.
4. W. C. W. Chan and S. M. Nie, *Science*, 1998, 281, 2016-2018.
5. M. Bruchez, M. Moronne, P. Gin, S. Weiss and A. P. Alivisatos, *Science*, 1998, 281, 2013-2016.
6. Z. Liu, S. Tabakman, K. Welsher and H. J. Dai, *Nano Res.* , 2009, 2, 85-120.
7. K. Welsher, Z. Liu, D. Daranciang and H. Dai, *Nano Lett.* , 2008, 8, 586-590.
8. P. Cherukuri, S. M. Bachilo, S. H. Litovsky and R. B. Weisman, *J. Am. Chem. Soc.*, 2004, 126, 15638-15639.
9. R. Y. Tsien, *Annu. Rev. Biochem.*, 1998, 67, 509-544.
10. R. M. Dickson, A. B. Cubitt, R. Y. Tsien and W. E. Moerner, *Nature*, 1997, 388, 355-358.
11. W. E. Moerner and D. P. Fromm, *Rev. Sci. Instrum.*, 2003, 74, 3597-3619.
12. W. E. Moerner and M. Orrit, *Science*, 1999, 283, 1670-1676.
13. A. P. Goodwin, S. M. Tabakman, K. Welsher, S. P. Sherlock, G. Prencipe and H. J. Dai, *J. Am. Chem. Soc.*, 2009, 131, 289-296.
14. R. Qiao and P. C. Ke, *J. Am. Chem. Soc.*, 2006, 128, 13656-13657.
15. R. H. Yang, J. Y. Jin, Y. Chen, N. Shao, H. Z. Kang, Z. Xiao, Z. W. Tang, Y. R. Wu, Z. Zhu and W. H. Tan, *J. Am. Chem. Soc.*, 2008, 130, 8351-8358.
16. N. W. S. Kam, M. O'Connell, J. A. Wisdom and H. J. Dai, *Proc. Natl. Acad. Sci. U. S. A.*, 2005, 102, 11600-11605.
17. M. Nirmal, B. O. Dabbousi, M. G. Bawendi, J. J. Macklin, J. K. Trautman, T. D. Harris and L. E. Brus, *Nature*, 1996, 383, 802-804.
18. A. M. Derfus, W. C. W. Chan and S. N. Bhatia, *Nano Lett.* , 2004, 4, 11-18.
19. C. F. Wu, T. Schneider, M. Zeigler, J. B. Yu, P. G. Schiro, D. R. Burnham, J. D. McNeill and D. T. Chiu, *J. Am. Chem. Soc.*, 2010, 132, 15410-15417.
20. Y. H. Jin, F. M. Ye, M. Zeigler, C. F. Wu and D. T. Chiu, *Acs Nano*, 2011, 5, 1468-1475.
21. C. Wu, B. Bull, C. Szymanski, K. Christensen and J. McNeill, *Acs Nano*, 2008, 2, 2415-2423.
22. Z. Hashim, P. Howes and M. Green, *J. Mater. Chem.*, 2011, 21, 1797-1803.
23. P. Howes, M. Green, J. Levitt, K. Suhling and M. Hughes, *J. Am. Chem. Soc.*, 2010, 132, 3989-3996.
24. F. C. Spano, *Annu. Rev. Phys. Chem.*, 2006, 57, 217-243.
25. J. Pecher and S. Mecking, *Chem. Rev.*, 2010, 110, 6260-6279.
26. A. Kaeser and A. P. Schenning, *Adv. Mater.*, 2010, 22, 2985-2997.
27. M. C. Baier, J. Huber and S. Mecking, *J. Am. Chem. Soc.*, 2009, 131, 14267-14273.
28. A. M. Smith and S. Nie, *J. Am. Chem. Soc.*, 2008, 130, 11278-11279.
29. I. L. Medintz, H. T. Uyeda, E. R. Goldman and H. Mattoussi, *Nat. Mater.*, 2005, 4, 435-446.
30. A. M. Smith, H. W. Duan, A. M. Mohs and S. M. Nie, *Adv. Drug Deliv. Rev.*, 2008, 60, 1226-1240.
31. T. Pellegrino, L. Manna, S. Kudera, T. Liedl, D. Koktysh, A. L. Rogach, S. Keller, J. Radler, G. Natile and W. J. Parak, *Nano Lett.* , 2004, 4, 703-707.

32. L. Song, C. A. Varma, J. W. Verhoeven and H. J. Tanke, *Biophys. J.*, 1996, 70, 2959-2968.
33. S. Hohng and T. Ha, *J. Am. Chem. Soc.*, 2004, 126, 1324-1325.
34. B. J. Schwartz, *Annu. Rev. Phys. Chem.*, 2003, 54, 141-172.
35. T. Q. Nguyen, I. B. Martini, J. Liu and B. J. Schwartz, *J. Phys. Chem. B*, 2000, 104, 237-255.
36. A. M. Smith, H. W. Duan, M. N. Rhyner, G. Ruan and S. M. Nie, *Phys. Chem. Chem. Phys.*, 2006, 8, 3895-3903.
37. T. Pons, H. T. Uyeda, I. L. Medintz and H. Mattoussi, *J. Phys. Chem. B*, 2006, 110, 20308-20316.
38. A. P. Alivisatos, *Science*, 1996, 271, 933-937.
39. C. A. Leatherdale, W. K. Woo, F. V. Mikulec and M. G. Bawendi, *J. Phys. Chem. B* 2002, 106, 7619-7622.
40. P. Kukura, M. Celebrano, A. Renn and V. Sandoghdar, *Nano Lett.* , 2009, 9, 926-929.
41. I. F. Sbalzarini and P. Koumoutsakos, *J. Struct. Biol.*, 2005, 151, 182-195.
42. L. H. Xiao, Y. X. Qiao, Y. He and E. S. Yeung, *J. Am. Chem. Soc.*, 2011, 133, 10638-10645.
43. L. H. Xiao, L. Wei, C. Liu, Y. He and E. S. Yeung, *Angew. Chem. Int. Ed. Engl.*, 2012, 51, 4181-4184.
44. A. M. Derfus, A. A. Chen, D. H. Min, E. Ruoslahti and S. N. Bhatia, *Bioconjug.Chem.*, 2007, 18, 1391-1396.
45. M. V. Yezhelyev, L. F. Qi, R. M. O'Regan, S. Nie and X. H. Gao, *J. Am. Chem. Soc.*, 2008, 130, 9006-9012.